

# Role of Electron–Electron Interactions on Spin Effects in Electron–Hole Recombination in Organic Light Emitting Diodes.

## Abstract

We extend our theory of electron–hole recombination in organic light emitting diodes to investigate the possibility that high energy singlet and triplet excited states with large electron–hole separations are generated in such processes, over and above the lowest singlet and triplet excitons. Our approach involves a time-dependent calculation of the interchain / intermolecular charge–transfer within model Hamiltonians that explicitly include electron–electron interactions between the  $\pi$ -electrons. We show that the electron–hole recombination reaction can be viewed as a tunneling process whose cross section depends on both the matrix element of the interchain part of Hamiltonian and the energy difference between the initial polaron–pair state and the final neutral states. There occurs a bifurcation of the electron–hole recombination path in each of the two spin channels that leads to the generation of both the lowest energy exciton and a specific high energy charge–transfer state, with the matrix elements favoring the lowest energy exciton and the energy difference factor favoring the higher energy state. The overall effect of the electron–electron interactions is to enhance the singlet:triplet yield ratio over the value of 0.25 predicted from statistical considerations that are valid only within noninteracting models.

# 1 Introduction

The fundamental electron-hole (e-h) recombination process in organic light emitting diodes (OLEDs) can be written as,



where  $P^\pm$  are charged polaronic states of the emissive molecule,  $G$  is the ground state of the neutral molecule,  $S$  is the singlet excited state and  $T$  the triplet excited state of the neutral molecule. Eq. 1 indicates that both singlet and triplet excitons are likely products of the e-h recombination process. The quantity that determines the efficiency of OLEDs is then the fraction of emissive singlets,  $\eta$ , that are formed in the above charge recombination process. Since electrons and holes are injected randomly in the device, only 25% of the initial polaron-pair states  $|P^+P^- \rangle$  are singlets. If it is now assumed that the rate constant for the e-h recombination in reaction 1 is equal for the singlet and the triplet channels (as would be true in the independent-electron limit), one arrives at a theoretical upper bound for  $\eta$  at 0.25. Many experimental studies, however, point to breaching of this upper bound in real systems [1–7] and  $\eta$  values considerably larger than 0.25 have been claimed.

At the same time though, there exists other experimental work that views these results with skepticism [8–10]. The latter authors argue that the value of  $\eta$  is decided entirely by the fraction of initial bound polarons  $|P^+P^- \rangle$  that are singlets, i.e., 0.25, and no further change in this quantity can take place, irrespective of the rates of the e-h recombination rates in the singlet and triplet channels in Eq. (1). Theoretical attempts to resolve this paradox recognize the important role of electron correlations in all cases, but can nevertheless be classified into two broad categories. In one, the focus has mostly been on the *lowest* singlet and triplet excited states, as in the independent electron model [11–14], and the calculation of the relative cross-sections of the e-h recombinations within the singlet and triplet channels were carried out in detail. Although the actual calculations are quite different within the different theoretical approaches within this category, the calculated yield of the lowest singlet exciton is greater than 0.25 in all cases. Within the second category of theoretical work, it is tacitly assumed (but not proved) that (i) the initial products of the e-h recombination are *higher energy* singlet and triplet states, and (ii) the yields of these excited singlets and triplets are in the ratio 1:3 (in conformity with the independent-electron statistics). Within this category of models it is the subsequent relaxations from the high energy states to the lowest singlet and triplet excitons that gives the change in the ratio of emissive singlets to triplets [15, 16]. As discussed later, from energetic considerations alone there is distinct possibility that the products of the e-h recombination reaction are the high energy excited states rather than the lowest excitons. The question therefore arises which of these two approaches, if any, describe best the e-h recombination in the real materials.

In view of these diverse experimental and theoretical results, we revisit our original work [13, 14] to investigate the possibility that the products of the e-h recombination reaction are high energy excited states, and to determine to what extent the singlet:triplet

yield ratio is affected by this. We show that in both the singlet and triplet channels, there exists strong likelihood of bifurcation of the reaction paths, with one path leading to the lowest exciton, the other leading to a specific excited state. Assuming now the applicability of Kasha's rule [17] within both spin channels (i.e., assuming that in both channels, the higher energy excited state decays to the lowest exciton in ultrafast time scale) one can in principle estimate the total yields of the lowest singlet and triplet states and the overall singlet:triplet ratio. This is what is attempted in the present paper.

In section 2 we present a brief review of the experimental results. In section 3 we present a mechanistic discussion of the e-h recombination for noninteracting electrons, with emphasis on the degeneracies that characterize this limit and the consequences thereof. We follow this with a summary on the the nature of excited states in conjugated polymers in section 4. These results are useful in obtaining physical understanding of the numerical results that we obtain for the e-h recombination. In sections 5 and 6, we present our theoretical model for the e-h recombination as well as detailed numerical results for various cases. In the Conclusion section we end with some basic issues that need to be addressed in the future and discuss our viewpoints regarding these issues.

## 2 Brief survey of experimental results

The basic difference between electroluminescence (EL) and photoluminescence (PL) in molecular materials lies in the initial process by which the excited state is formed. Independent of this step, in both cases, as per the Kasha rule [17] fluorescent emission occurs from the lowest excited singlet electronic state (with very few exceptions). This is because rapid internal conversion funnels higher excited states to the lowest excited state of the same spin symmetry, whenever the equilibrium geometries of the initial and final excited states are not very different. Thus the cross-section for the final process of light emission is nearly the same in both EL and PL. However, while the formation of the emissive species, the singlet optical exciton, has a quantum efficiency (QE) of nearly 1 in the PL process, this QE is  $\eta$  in the case of EL. Hence, the ratio of the EL to PL efficiency provides a lower bound on  $\eta$  in the e-h recombination in the EL process. Using this principle, experimentally  $\eta$  has been found to range from  $\approx 0.25$  to 0.66 in different materials [1, 2, 4]. In OLEDs containing molecular components as the emissive species, such as aluminum tris (8-hydroxy quinoline) ( $\text{Alq}_3$ ),  $\eta$  has been determined to be close to the independent-electron statistical value [8,9]. On the other hand, considerably larger  $\eta$  of 0.45 has been claimed in derivatives of poly (para phenylene vinylene) (PPV) by Cao *et al.* [1] and Ho *et al.* [2].  $\eta$  has also been measured by photoinduced absorption detected magnetic resonance (PADMR) [4,6]. In this technique a magnetic field of about 0.1 Tesla is applied to Zeeman split the spin-1/2 states of the charged polarons at a temperature of about 20 K. Application of an intense microwave to match the Zeeman splitting leads to equal populations of the up and down spin states. This in turn would lead to higher probability of two neighboring polarons of opposite charge having

antiparallel spin orientations than parallel spin orientations. Thus, the recombination will yield fewer triplets than in the absence of a field and a saturating microwave, resulting in attenuation of the triplet absorption in the PADMR experiment. From measurement of this attenuation, it is possible to calculate  $\eta$ . Wohlgenannt *et al.* [4,6] have determined  $\eta$  for a large number of polymeric materials this way and have found it to be strongly material dependent; in all the cases they studied,  $\eta$  was determined to be larger than 0.25. More recently, Wilson *et al.* [3] and Wohlgenannt *et al.* [6] have shown that  $\eta$  varies with conjugation length, from 0.25 for small molecules to considerably larger for long chain oligomers. These results are in contradiction with the claim in reference [9] that in electroluminescent devices with MEH-PPV as the emissive material the singlet fraction is  $(20 \pm 4)\%$ .

Increase in the population of polaron pairs with antiparallel spins under resonance condition also implies formation of a higher fraction of singlet excitons. Monitoring EL intensity under resonance conditions (ELDMR) should give an enhancement consistent with the decrease in PA intensity under the same conditions. This has indeed been observed by Segal *et al.* [9] as well as Li *et al.* [10] in Alq<sub>3</sub>. Since estimates based on other measurements give  $\eta \sim 0.25$  for Alq<sub>3</sub> [8,9], Li *et al.* attribute this increase in EL to reduced polaron population under resonance leading to reduced quenching of the singlet excitons [10]. Reduced polaron population results, however, from increased recombination process and hence increased population of singlet excitons. Thus in polymeric materials, the enhanced ELDMR could be both due to higher rate of recombination process and reduced rate of quenching of the singlet excitons.

Finally a recent experimental paper by Lin *et al.* has claimed that  $\eta$  can be *smaller* than 0.25 in LED devices under low electric field [18]. This work, however, has been severely criticized by authors who have pointed out that the experiments were carried out at room temperature, and the absorption spectrum assigned to triplets by Lin *et al.* was actually due to charged polarons [19,20]. Furthermore, the critical assumption in the model, namely, that no triplet states exist between the conduction band edge triplet and the lowest triplet is not borne by the exact triplet spectrum calculated for long conjugated chains [21] using the widely accepted Pariser–Parr–Pople model [22].

### 3 Two-level picture of e-h recombination

In view of what follows, we discuss here briefly the recombination reaction (1) for independent electrons (Hückel model). The electronic structures of all the components in Eq. (1) are given by single molecular configurations in this limit, and for arbitrary chain lengths or molecular sizes, only the highest occupied and lowest unoccupied molecular orbitals (HOMO and LUMO) are relevant. Each component of reaction (1) can therefore be described within a two-level scheme, as shown in Fig. 1. The total energy of the initial state  $|P^+ \cdot P^- \rangle$  and the final state  $|G \cdot S/T \rangle$  in Fig. 1 are identical. Hence if we view the e-h recombination as a tunneling process, there occurs resonant tunneling from the initial polaronic states to the final neutral states, if the matrix element of

the perturbation (corresponding to the transfer term which causes an electron to hop between the conjugated chains) connecting the initial and final states are nonzero. The matrix elements  $\langle G \cdot S | H | P^+ P^- \rangle_S$  and  $\langle G \cdot T | H | P^+ P^- \rangle_T$ , where  $|P^+ P^- \rangle_S$  and  $|P^+ P^- \rangle_T$  are singlet and triplet polaron-pair species, are identical for arbitrary interchain hopping and hence the tunneling probability is the same in the singlet and the three triplet channels. This quantum resonant tunneling picture leads us to  $\eta = 0.25$ . Notice that this requires the strict degeneracy

$$E(P^+) + E(P^-) = E(G) + E(S/T) \quad (2)$$

where the energy  $E$  in each case refers to the total energy of the state in question. If for any reason these equalities are not obeyed, in particular if  $E(S) \neq E(T)$  there is no reason to have  $\eta = 0.25$ .

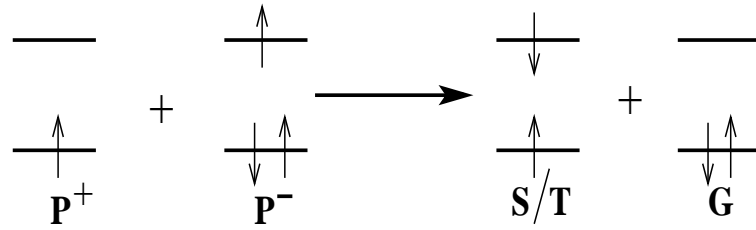


FIG. 1. *The HOMO and LUMO orbital occupancies for the initial polaronic pair state and the final neutral states for the total z-component of the spin  $M_s=0$ .*

## 4 Excited states in conjugated polymers

We briefly review here the nature of the excited states in conjugated polymers within correlated electron models. This will be useful in understanding the bifurcation of the e-h recombination paths (1) mentioned in the above.

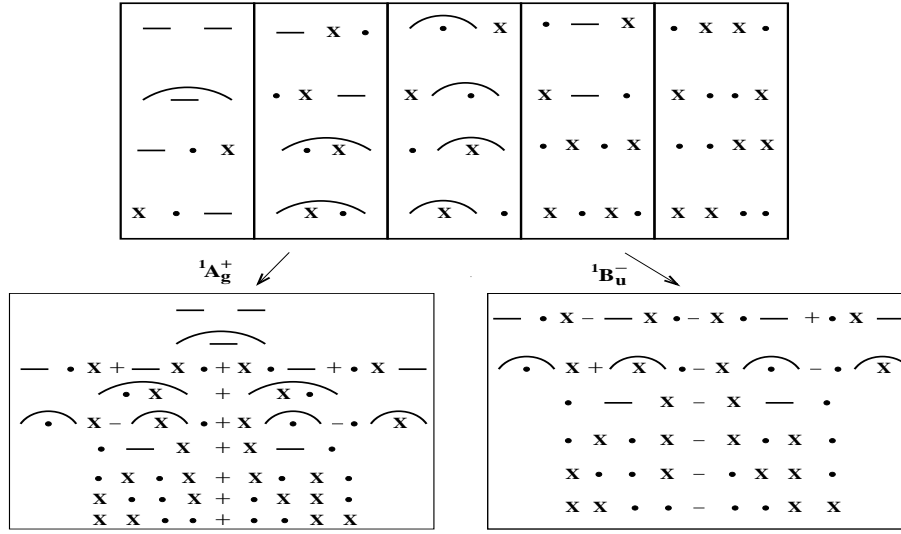
The noninteracting electrons description of conjugated polymers is based on the  $\pi$ -electron Hückel model. The Hückel molecular orbitals (HMOs) are obtained as linear combinations of the atomic  $2p_z$  orbitals, one at each carbon atom in conjugation. Usual quantum chemical approaches that go beyond Hückel theory use the HMOs as the starting point and include electron correlations via a configuration interaction (CI) scheme by using a restricted number of excited HMO configurations such as the singly excited and the doubly excited configurations in the singles and doubles CI (SDCI) approach. However, when the strength of repulsion between two electrons occupying the same  $2p_z$  orbital is comparable to the energy difference between the LUMO and the HOMO, it is preferable to start with the electron configurations in the atomic orbital (AO) basis. This is particularly important in the polymer limit since approaches such as SDCI are not size-consistent and size-consistent techniques such as perturbation

methods do not converge in the regime of intermediate correlations. The guiding factors in this regime would be the physical insights developed from a real space or AO picture. In this section we will illustrate how this picture helps in understanding the excitations of a conjugated polymer chain.

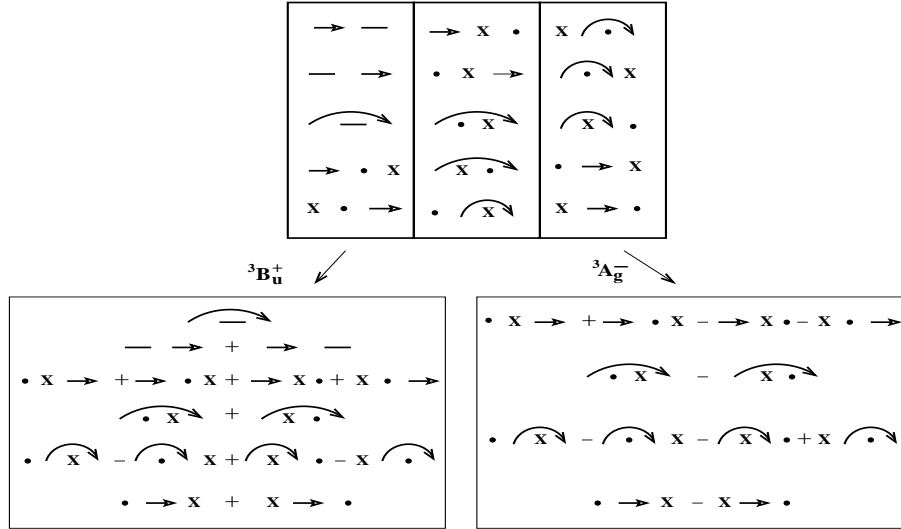
We begin with the analysis of the simple case of butadiene with four  $2p_z$  orbitals ( $N=4$ ) in conjugation. The number of electrons  $N_e$  occupying the  $N$  orbitals is also 4. The models we deal with are nonrelativistic (since spin-orbit interactions are negligible) and hence total spin,  $S$ , as well as the  $z$ -component of total spin,  $M_S$ , are well defined. We can write 36 distinct (linearly independent) electron configurations corresponding to  $M_S = 0$  for the case of  $N_e = N = 4$ . Constructing basis functions with fixed total spin, such as  $S = 0$  singlet basis functions or  $S = 1$  triplet basis functions is nontrivial. The approach that has proved to be useful and physically appealing has been to use valence bond (VB) functions [23], which are linear combinations of the Slater determinants corresponding to different MO configurations. The VB basis states are completely defined if (i) the orbital occupancies by electrons are defined and (ii) the spin-pairing among the singly occupied orbitals are provided. VB singlets are represented by lines connecting the orbital pair (see Fig. 2 and discussion below). For VB basis with  $S \neq 0$  and  $M_S = S$ , besides the singlet pairings, it is also necessary to specify the  $2S$  AOs with parallel spin occupancies. Within our VB theory such sites are connected by a triplet bond, represented by arrows (see Fig. 2).

In Figs. 2 (a) and (b) we show the twenty singlet and fifteen triplet VB diagrams for  $N = N_e = 4$ . Linear chains have mirror plane as well as inversion symmetries, implying that all basis functions as well as eigenstates can be classified as having even spatial parity ( $A_g$ ) and odd spatial parity ( $B_u$ ). The bipartite nature of linear polyenes (as well as most conjugated polymers) also implies charge-conjugation symmetry; thus each spatial symmetry subspace can be further partitioned into even and odd charge-conjugation symmetries, giving four different symmetry subspaces overall. We have given in Fig. 2(a) the VB basis functions, – superpositions of VB diagrams, – that form the  $S = 0$   $A_g^+$  and  $B_u^-$  subspaces (the other two subspaces,  $A_g^-$  and  $B_u^+$ , are not shown). Similarly in Fig. 2(b) we have shown the  $B_u^+$  and  $A_g^-$   $S = 1$  basis functions.

Broadly, the basis functions in Figs. 2(a) and (b) can be classified as covalent, i.e., consisting of VB diagrams in which all atoms are singly occupied (the first two basis functions in the  $^1A_g^+$  subspace, as well as the first two basis functions in the  $^3B_u^+$  subspace), and ionic, with at least one doubly occupied site and one empty site (all other basis functions in Figs. 2). The ionic basis functions can be further classified into singly ionic (with one doubly occupied and one empty site), doubly ionic (with two doubly occupied and two empty sites), and so on (higher ionicities occurring in  $N_e=N > 4$ ). The ground state lies in the  $A_g^+$  subspace (and henceforth is referred as the  $1^1A_g^+$ ), and with increasing electron-electron interactions, the ionicity of the ground state decreases and the wavefunction is more strongly dominated by the covalent basis functions (since the on-site part of the electron correlations raise the energies of basis functions with double occupancies). Optical excitation from this state is to the lowest  $^1B_u^-$  state (here-



(a)



(b)

FIG. 2. The VB basis states for singlets and triplets for butadiene. Each cross (X) represents  $2p_z$  orbital at the site occupied by two electrons, a dot (.) represents an empty orbital and a line (arrow) between two sites represents singlet (triplet) spin-pairing of the singly occupied  $2p_z$  orbitals at the sites. In (a) the twenty singlet VB diagrams yielding nine symmetrized singlet basis in the  ${}^1A_g^+$  and six symmetrized singlet basis in the  ${}^1B_u^-$  subspaces are shown. The ground state lies in the  ${}^1A_g^+$  subspace while the optically allowed excitations from the ground state lie in the  ${}^1B_u^-$  subspace. Two other subspaces corresponding to  ${}^1A_g^-$  and  ${}^1B_u^+$  subspaces are not shown. In (b) the fifteen triplet VB diagrams, the six basis states in the  ${}^3B_u^+$  subspace, and the four basis states in the  ${}^3A_g^-$  subspace are shown. The lowest triplet lies in the  ${}^3B_u^+$  subspace.

after  $1^1B_u^-$ ), which, as seen from Fig. 2(a), is necessarily ionic as there exist no covalent VB diagrams in the  $1^1B_u^-$  subspace. In contrast, the lowest triplet states in the  $3^1B_u^+$  subspace again have strong covalent contributions, and hence are lower in energy than the  $1^1B_u^-$ . There exist a “band” of such triplet states between the  $1^1A_g^+$  and the  $1^1B_u^-$  in the long chain limit. The  $3^1B_u^+$  is higher in energy than the  $1^1A_g^+$ , since while there can be charge-transfer delocalization across an arbitrary singlet bond, there is no such charge-transfer across triplet bonds. From the physical natures of the basis functions then, it is clear that several of the lowest triplets will occur below the  $1^1B_u^-$ .

If the electron correlations include intersite Coulomb interactions over and above on-site correlations, singly ionic VB basis functions with neighboring double occupancy (particle) and vacancy (hole) (the third basis function in the  $1^1A_g^+$  subspace and the first basis function in the  $1^1B_u^-$  subspace) have lower energy than basis functions in which the double occupancy and the vacancy are further away. In the long chain limit there are many more (practically infinite) basis functions that belong to the latter class and few with short range separations between the double occupancy and the vacancy. We see therefore that for realistic strong Coulomb interactions that characterize conjugated polymers there will be a strong tendency for formation of excitons, with a few of the states dominated by ionic VB functions with small separations between the double occupancy and the vacancy splitting off from the continuum of singly ionic states.

The above conjectures based on the physical nature of the VB basis functions have been substantiated by numerical calculations by several groups [24–27] and is also supported by experiments [24, 28–36]. In Fig. 3 we have shown the schematic energy spectrum of conjugated polymers. The singlet and triplet exciton states below the conduction band edge that are labeled as  $m^1A_g^+$  and  $m^3A_g^-$  have been discussed extensively in the context of optical nonlinearity and are characterized by very large transition dipole couplings to the  $1^1B_u^-$  and  $3^1B_u^+$  states respectively [24–27]. Energetically, the  $m^1A_g^+$  is degenerate with the  $m^3A_g^-$  at the level of singles-CI [25] and very slightly above the  $m^3A_g^-$  within exact calculations [37]. Still higher energy singlet and triplet states with large transition dipoles to the  $m^1A_g^+$  and  $m^3A_g^-$  states are the  $n^1B_u^-$  and  $n^3B_u^+$  [24–26], also included in Fig. 3. The  $n^1B_u^-$  lies at the edge of the continuum threshold, as has been shown from earlier calculations [24–26]. The  $n^3B_u^+$  has not been discussed previously. We have calculated the energy of this state exactly for a large range of parameters (see below) and have found in all cases this state to be nearly degenerate with the  $m^3A_g^-$  and invariably below the  $n^1B_u^-$ . Although the bulk of the energetics calculations are for linear chain polyacetylenes and polydiacetylenes [24–26], work by different groups have indicated that the same basic energy level scheme applies also to conjugated polymers with aromatic groups, in the energy region up to and including the conduction band threshold [38–40]. It is natural to assume that the ground state of the polaron pair formed in the OLEDs,  $|P^+P^- \rangle$  is just at the bottom of the conduction band edge. This state is also included in Fig. 3, where we have made no distinction between  $|P^+P^- \rangle_s$  and  $|P^+P^- \rangle_t$ , as the energy difference between the singlet and triplet polaron-pair states is tiny [41] and would be invisible on the scale of Fig. 3.



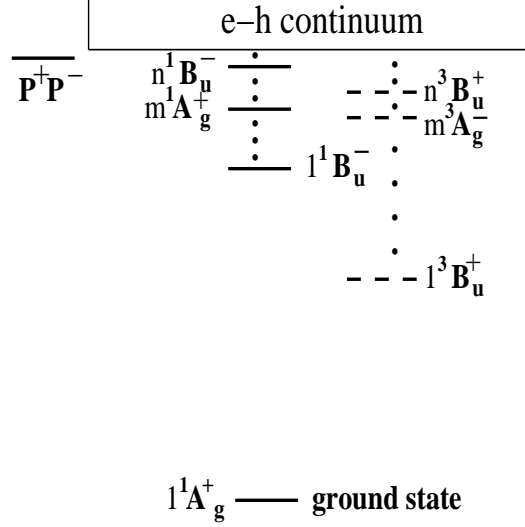


FIG. 3. *Schematic excitation spectrum of a conjugated polymer. Dots indicate that there are several excitations between the labeled states.*

## 5 Correlated electron theory of e-h recombination

Our goal in this section is to lay out the formalism for the detailed calculations of relative formation rates of singlet and triplet excitons starting from an oppositely charged polaron pair (see reaction (1)), in view of the correlated electron description of the electronic structure of  $\pi$ -conjugated polymers (see Fig. 3). In contrast to our earlier work [13, 14], we recognize at the outset that e-h recombination can generate S and T states at energies higher than the lowest energy excitons. We calculate the yields to all such states under different conditions using the techniques developed in [13, 14]. Our procedure consists in computing the time-dependent evolution of oppositely charged polyene molecules under the influence of the composite two-chain Hamiltonian, as discussed below. As we limit ourselves to calculations based on the rigid bond approximation and small finite molecules, we assume that all high energy singlets and triplets decay in ultrafast times to the  $1^1B_u^-$  and  $1^3B_u^+$ , respectively. We believe that this assumption is valid for the real systems [21].

### 5.1 The model system

Our model system consists of two polyene chains of equal lengths that lie directly on top of each other, separated by 4 Å. We consider the charge recombination process of Eq. 1, and there are two possible initial states: (i) a specific chain (say chain 1) is positively charged, with the other (chain 2) having negative charge, a configuration that hereafter we denote as  $P_1^+P_2^-$ , where the subscripts 1 and 2 are chain indices, or (ii) the superposition  $P_1^+P_2^- \pm P_2^+P_1^-$ , in the same notation. In our calculations we have

chosen the first as the proper initial state, since experimentally in the OLEDs the symmetry between the chains is broken by the external electric field (we emphasize that the consequence of choosing the symmetric or antisymmetric superposition can be easily predicted from all our numerical calculations that follow). Even with initial state (i), the final state can consist of both  $G_1 \cdot S_2$  and  $G_2 \cdot S_1$  in the singlet channel. The same is true in the triplet channel, i.e., either of the two chains can be in the ground (excited) state. Hereafter we will write the initial states as  $|i_S\rangle$  and  $|i_T\rangle$ , where the subscripts S and T correspond to spin states  $S = 0$  and 1. We consider only the  $M_S = 0$  triplet state. In the absence of an external magnetic field the e-h recombination reaction rate for all three triplet channels with different  $M_S$  are the same. The initial states are simply the product states with appropriate spin combinations,

$$|i_S\rangle = 2^{-1/2}(|P_{1,\uparrow}^+\rangle|P_{2,\downarrow}^-\rangle - |P_{1,\downarrow}^+\rangle|P_{2,\uparrow}^-\rangle) \quad (3)$$

$$|i_T\rangle = 2^{-1/2}(|P_{1,\uparrow}^+\rangle|P_{2,\downarrow}^-\rangle + |P_{1,\downarrow}^+\rangle|P_{2,\uparrow}^-\rangle) \quad (4)$$

The overall Hamiltonian for our composite two-chain system consists of an intrachain part  $H_{\text{intra}}$  and an interchain part  $H_{\text{inter}}$ .  $H_{\text{intra}}$  describes individual chains within the Pariser-Parr-Pople (PPP) Hamiltonian [22] for  $\pi$ -electron systems, written as,

$$H_{\text{intra}} = - \sum_{\langle ij \rangle, \sigma} t_{ij} (a_{i,\sigma}^\dagger a_{j,\sigma} + \text{H.C.}) + \sum_i \epsilon_i n_i + \sum_i U_i n_{i,\uparrow} n_{i,\downarrow} + \sum_{i>j} V_{ij} (n_i - z_i)(n_j - z_j) \quad (5)$$

where  $a_{i,\sigma}^\dagger$  creates a  $\pi$ -electron of spin  $\sigma$  on carbon atom  $i$ ,  $n_{i,\sigma} = a_{i,\sigma}^\dagger a_{i,\sigma}$  is the number of electrons on atom  $i$  with spin  $\sigma$  and  $n_i = \sum_\sigma n_{i,\sigma}$  is the total number of electrons on atom  $i$ ,  $\epsilon_i$  is the site energy and  $z_i$  are the local chemical potentials. The hopping matrix element  $t_{ij}$  in the above are restricted to nearest neighbors and in principle can contain electron-phonon interactions, although a rigid bond approximation is used here.  $U_i$  and  $V_{ij}$  are the on-site and intrachain intersite Coulomb interactions.

We use standard parameterizations for  $H_{\text{intra}}$ . The hopping integrals for single and double bonds are taken to be 2.232 eV and 2.568 eV, respectively and all site energies, for simple polyenes with all sites equivalent, are set to zero. We choose the Hubbard interaction parameter  $U_C$  for carbon to be 11.26 eV, and for the  $V_{ij}$  we choose the Ohno parameterization [42],

$$V_{ij} = 14.397 \left[ \left( \frac{28.794}{U_i + U_j} \right)^2 + r_{ij}^2 \right]^{-\frac{1}{2}} \quad (6)$$

where the distance  $r_{ij}$  is in Å,  $V_{ij}$  is in eV and the local chemical potential  $z_C$  for  $sp^2$  carbon is one. It should be noted then when heteroatoms like nitrogen are present,

the on-site correlation energy, the site energy and the local chemical potential could be different from those for carbon [13]. For  $H_{\text{inter}}$ , we choose the following form,

$$\begin{aligned}
H_{\text{inter}} = & -t_{\perp} \sum_{i,\sigma} (a_{i\sigma}^{\dagger} a'_{i,\sigma} + \text{H.C.}) + \\
& + X_{\perp} \sum_{i,\sigma} (n_i + n'_i) (a_{i\sigma}^{\dagger} a'_{i,\sigma} + \text{H.C.}) + \\
& \sum_{i,j} V_{i,j} (n_i - z_i) (n'_j - z'_j)
\end{aligned} \tag{7}$$

In the above, primed and unprimed operators refer to corresponding sites on different chains. Note that the interchain hopping  $t_{\perp}$  is restricted to nearest interchain neighbors. The interchain Coulomb interaction  $V_{i,j}$ , however, includes interaction between any site on one chain with any other site on the other chain. In addition to the usual one-electron hopping that occurs within the zero differential overlap approximation we have also included a many-electron site charge-bond charge repulsion  $X_{\perp}$  (operating between nearest interchain neighbors only) that consists of multicenter Coulomb integrals [22,43]. This term should also occur within  $H_{\text{intra}}$ , but is usually ignored there because of its small magnitude, relative to all other terms. In contrast, the  $t_{\perp}$  in  $H_{\text{inter}}$  is expected to be much smaller, and  $X_{\perp}$  cannot be ignored in interchain processes, especially at large interchain separations [44]. We have done calculations for both  $X_{\perp} = 0$  and  $X_{\perp} \neq 0$ .

## 5.2 Time-evolution of the polaron pair state

Our approach consists in calculating the time-evolution of the initial states  $|i_S\rangle$  and  $|i_T\rangle$  [see Eqs. (3) and (4)] under the influence of the full Hamiltonian, and then evaluating the overlaps of the time-evolved states with all possible final states  $|f_S\rangle$  and  $|f_T\rangle$  of the individual neutral chains. In OLEDs, the  $P^{\pm}$  are created at opposite ends of the device and they execute hopping motion towards each other under the influence of an external electric field ( $P^{\pm} + G \rightarrow G + P^{\pm}$ ). The polaron wavefunctions remain unperturbed throughout this process, until they are within the radius of influence of each other. We define this particular instant as time  $t = 0$ , and we visualize that the interchain interactions  $H_{\text{inter}}$  are “switched on” suddenly from zero at this time. The intermolecular charge-transfer (CT) hereafter is rapid (a few to several tens of femtoseconds, for realistic interchain hopping  $t_{\perp}$ , see below). It is the ultrashort timescale of this CT process that justifies the choice of our initial state.

In principle, given a Hamiltonian, propagation of any initial state is easily achieved by solving the time-dependent Schrodinger equation. One could use the interaction picture to separate the nontrivial evolution of the initial state from the trivial component which occurs as a result of the evolution of the product of the eigenstates of the Hamiltonian of the subsystems. In the context of the many-body PPP Hamiltonian such an approach is difficult to implement numerically. This is because the total number of eigenstates for the two-chain system is very large: the number of such states for two chains of six carbon atoms each is 853,776 in the  $M_s = 0$  subspace. Obtaining

all the eigenstates of the two-component system and expressing the matrix elements of  $H_{\text{inter}}$  in the basis of these eigenstates is therefore very intensive computationally. It is simpler to calculate the time evolution in the Schrodinger representation, determine the time-evolved states, and project them on to the desired final eigenstates (for instance,  $|1^1A_g\rangle_1|1^1B_u\rangle_2$ ). This is the approach we take.

Henceforth we refer to the initial states  $|i_S\rangle$  and  $|i_T\rangle$  collectively as  $\Psi(0)$  and the time-evolved states as  $\Psi(t)$ . In principle, the time evolution can be done by operating on  $\Psi(0)$  with the time evolution operator,

$$U(0, t) = \exp(-iHt) \quad (8)$$

where  $H$  is the total Hamiltonian  $H_{\text{intra}} + H_{\text{inter}}$ . This approach would, however, require obtaining a matrix representation of the exponential time evolution operator, which again requires the determination of the prohibitively large number of eigenstates of the composite two-chain system. We can avoid this problem by using small discrete time intervals and expanding the exponential operator in a Taylor series, and stopping at the linear term. Such an approach, however, has the undesirable effect of spoiling unitarity, and for long time evolutions would lead to loss of normalization of the evolved state. The way around this dilemma has been proposed and used by others [45, 46] in different contexts and involves using the following truncated time-evolution scheme,

$$(1 + iH\frac{\Delta t}{2})\Psi(t + \Delta t) = (1 - iH\frac{\Delta t}{2})\Psi(t) \quad (9)$$

In the above equation, on the left hand side, we evolve the state at time  $(t + \Delta t)$  backward by  $\Delta t/2$  while on the right hand side, we evolve the state at time  $t$  forward by  $\Delta t/2$ . By forcing these two to be equal, we ensure unitarity in the time evolution of the state. It can be seen easily that this time evolution which is accurate to  $\frac{\Delta t^2}{2}$  is unitary. For a given many-body Hamiltonian and initial state, the right hand side of Eq. 9 is a known vector in the Hilbert space of the two-chain Hamiltonian. The left hand side corresponds to the action of a matrix on an as yet unknown vector, that is obtained by solving the above set of linear algebraic equations.

After each evolution step, the evolved state is projected onto the space of neutral product eigenstates of the two-chain system. The relative yield  $I_{mn}(t)$  for a given product state  $|m, n\rangle = |m\rangle_1|n\rangle_2$  is then obtained from,

$$I_{mn}(t) = |\langle\Psi(t)|m, n\rangle|^2 \quad (10)$$

In our case the states  $|m, n\rangle$  can be any of the final states of interest, viz.,  $|(1^1A_g)_1(1^1B_u)_2\rangle$ ,  $|(1^1A_g)_1(1^3B_u)_2\rangle$ , etc. It is for efficient calculations of the overlaps (while at the same time maintaining spin purity) in Eq. 10 that we transfer our exact eigenstates of the neutral system in the VB basis to the total  $M_S$  basis. We emphasize that  $I_{mn}(t)$  is a measure of the yield of the state  $|m, n\rangle$  at time  $t$  and is not a cross-section.

## 6 Numerical Results

We first present the results of our calculations of recombination dynamics for pairs of ethylenes, butadienes and hexatrienes within the noninteracting Hückel model ( $U_i = V_{ij} = X_\perp = 0$ ) and the interacting PPP model. These results have already been discussed in detail in reference [4], and hence our presentation will be brief. Our calculations here clearly indicate that the yield of the lowest singlet exciton is considerably larger than that of the lowest triplet exciton within the PPP Hamiltonian. As already discussed in section I, however, it is not necessary that the reaction products of the e-h recombination reaction are limited to the lowest excitations when e-e interactions are nonzero. A thorough search within the PPP model has, however, not detected significant yield of any other excited state [4]. We discuss why this might be a consequence of the small sizes of our model systems. We then present new results of calculations with  $H_{\text{intra}}$  as the simple Hubbard Hamiltonian ( $V_{ij} = 0$ ) and an extended Hubbard Hamiltonian with short-range intersite Coulomb interactions. In spite of the obvious limitations of our finite size calculations, a mechanism of e-h recombination appears to emerge from our work. We are able to show that in both singlet and triplet channels, there occurs a bifurcation of the e-h recombination paths, with one branch leading to the lowest  $1^1B_u$  ( $1^3B_u$ ) exciton, the other leading to the formation of the  $n^1B_u$  ( $n^3B_u$ ) higher energy CT states. The overall S:T ratio then depends on the relative weights of the two branches in each spin channel, but the fractional singlet exciton yield continues to be greater than 0.25.

### 6.1 Dynamics in the Hückel Model

While there is no difference in energy between singlets and triplets in the Hückel Model, it is nevertheless possible to have spin singlet and triplet initial states  $|i_S\rangle$  and  $|i_T\rangle$ , as well as singlet and triplet final states. In Fig. 4 we show the yield for the e-h recombination in the singlet channel, for pairs of ethylenes, butadienes and hexatrienes. The yields for the triplet channels are not shown separately in this case, – we have ascertained that these are identical to those in the singlet channel in this case, as expected. These calculations are for  $t_\perp = 0.1$  eV,  $X_\perp = 0$  within Eq. 7. We note that the yields  $I_{mn}(t)$  oscillate with time. This is to be expected within our purely electronic Hamiltonian, within which an electron or hole jumps back and forth between the two molecular species. These oscillations are the analogs of the Rabi oscillations [47, 48] that occur upon the stimulation of a system with light, where absorption of light can occur only with nonzero damping. Within our purely electronic Hamiltonian, complete transition to the final states can only occur in the presence of damping (for example, radiative and nonradiative relaxations of the final states), that has not been explicitly included in our Hamiltonian. The frequency of oscillation is higher for larger intermolecular transfer integral  $t_\perp$ , as expected. The frequency of the oscillation also depends upon the size of the molecule and is lower for larger molecules. The equalities in the yields of the singlet and triplet excited states found numerically conforms to the simple free spin

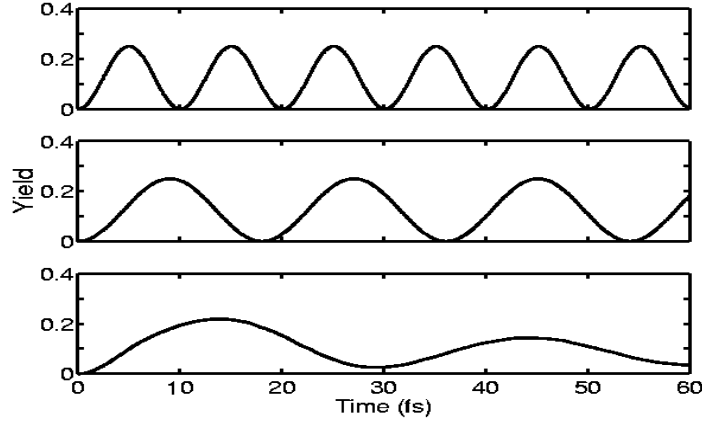


FIG. 4. *Yield in the singlet channel as a function of time, for pairs of ethylenes (top panel), butadienes (middle panel), and hexatrienes (bottom panel), within the Hückel model ( $U = V_{ij} = X_{\perp} = 0$ ).*

statistics prediction that the probability of singlet and triplet formation are equal in the e-h recombination process with  $M_s = 0$  as the initial state. Since the  $M_s = \pm 1$  cases always yield triplets, the spin statistics corresponding to 25% singlets and 75% triplets is vindicated in this case.

## 6.2 Dynamics in the PPP model

The results presented in this subsection are for interchain  $V_{i,j}$  calculated using the Ohno parameters, and interchain hopping  $t_{\perp} = 0.1$  eV. We present the results for both  $X_{\perp} = 0$  and 0.1 eV. The top left and top right plots in Fig. 5 show the yield  $I_{mn}(t)$  in the singlet and triplet channels for pairs of ethylenes, butadienes and hexatrienes, respectively, for the case of  $X_{\perp} = 0$ . The same results are shown in bottom left and bottom right plots for  $X_{\perp} = 0.1$  eV.

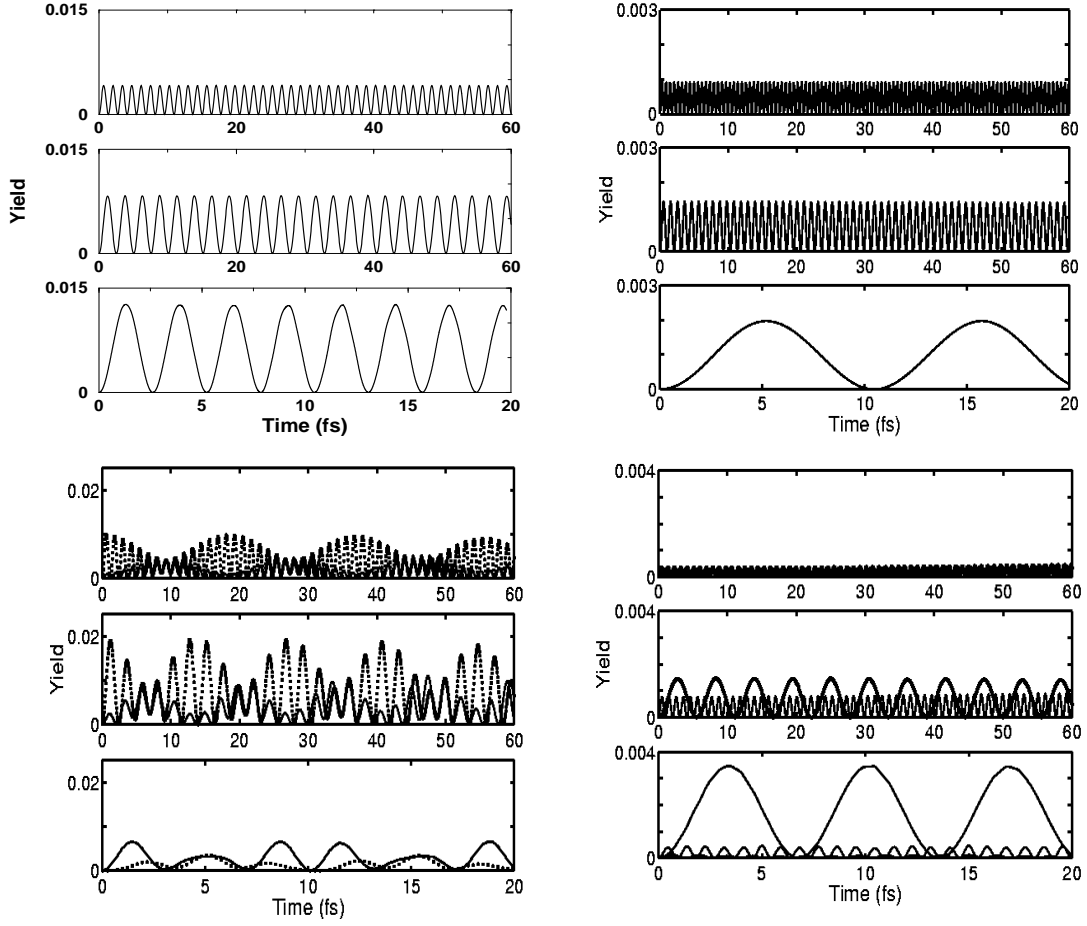


FIG. 5. Yields in the singlet and triplet channels within the PPP Hamiltonian. In all four cases the top panel corresponds to pair of ethylenes, the middle panel to pairs of butadienes, and the bottom panel to pairs of hexatrienes. Top left: singlet channel,  $t_{\perp} = 0.1\text{eV}$ ,  $X_{\perp} = 0$ . Top right: triplet channel,  $t_{\perp} = 0.1\text{eV}$ ,  $X_{\perp} = 0$ . Bottom left: singlet channel,  $t_{\perp} = 0.1\text{eV}$ ,  $X_{\perp} = 0.1\text{eV}$ . Bottom right: triplet channel  $t_{\perp} = 0.1\text{eV}$ ,  $X_{\perp} = 0.1\text{eV}$ . Evolution in case of hexatrienes is tracked for 20 fs while in other cases, the evolution is tracked for 60 fs. Significant yields in singlet channel occurs only for final states  $|(^1A_g^+)_1(^1B_u^-)_2\rangle$  and  $|(^1B_u^-)_1(^1A_g^+)_2\rangle$ , between which the yields are identical for  $X_{\perp} = 0$  but different for  $X_{\perp} \neq 0$ . Similar asymmetry is observed also in the triplet channels for  $X_{\perp} \neq 0$ .

The differences from the Hückel model results are the following. First, the yields  $I_{mn}(t)$  in both the singlet and triplet channels are considerably reduced in the PPP model. Second, the  $1^1B_u^-$  yield is now substantially higher than that of the  $1^3B_u^+$  in all cases. Finally, the observed higher yield of the singlet exciton is true for both  $X_{\perp} = 0$  and  $X_{\perp} \neq 0$ . This is in contradiction to the results obtained in references [11,12], which ignore the energy difference between the  $1^1B_u^-$  and the  $1^3B_u^+$ . The only consequence of nonzero  $X_{\perp}$  is the asymmetry between the yields of  $(^1A_g)_1(^1B_u)_2$  and  $(^1A_g)_2(^1B_u)_1$  in the singlet channels, and a similar asymmetry in the triplet channels. The overall conclusion that emerges from the results of the plots in Figs. 5 is that nonzero electron-electron

interactions substantially enhances  $\eta$ .

### 6.3 Finite size effects and their origin

In what follows we will take the ground state energy  $E(1^1A_g)$  to be zero. In the infinite chain limit the sum total of the energies of the two oppositely charged polarons,  $E(P^+) + E(P^-)$ , must be equal to the lowest singlet continuum band state in the neutral chain, independent of Coulomb interactions. Within the rigid band simple Hubbard model ( $V_{ij} = \epsilon_i = 0$  in Eq. 5) as  $H_{\text{intra}}$ , this implies that in the long chain limit  $E(P^+) + E(P^-) = E(1^1B_u)$ . For nonzero intersite Coulomb interactions that are large enough to create an excitonic energy spectrum,  $E(P^+) + E(P^-) = E(n^1B_u)$  in the long chain limit. Neither of these equalities are obeyed in short chains. In Table 1, we have listed  $E(P^+) + E(P^-)$  and  $E(1^1B_u)$  for the simple Hubbard model with  $t_{ij} = t(1 \pm \delta)$ ,  $t = 1$ , and  $\delta = 0.2$  for many different  $U$ , for  $N = 6$ . All quantities are in units of  $t$ . We have also included here  $E(n^3B_u)$ , defined in section 4. In all cases  $E(1^1B_u)$  is significantly larger than  $E(P^+) + E(P^-)$ , with the difference increasing with  $U$ . For nonzero intersite Coulomb interactions,  $E(n^1B_u)$  is similarly significantly higher than  $E(P^+) + E(P^-)$ , as shown in Table 2 for  $N = 6$ , although the difference in energy decreases with increasing interaction strength, due to localization. For sufficiently large Coulomb interactions,  $E(n^3B_u)$  occurs below  $E(P^+) + E(P^-)$  for  $N = 6$  within the extended Hubbard model.

Table 1:  $N = 6$  energetics within the simple Hubbard model. All energies are in units of  $t$ .

$U$	$E(P^+) + E(P^-)$	$E(1^1B_u)$	$E(n^3B_u)$
2	1.75	1.99	2.94
4	2.70	3.05	3.58
6	4.08	4.48	4.84
8	5.70	6.12	6.40
10	7.45	7.89	8.12
12	9.28	9.72	9.92
20	16.92	17.38	17.50



Table 2:  $N = 6$  energetics within the extended Hubbard model. All energies are in units of  $t$ .

U	V	$E(P^+) + E(P^-)$	$E(n^1B_u)$	$E(n^3B_u)$
10	3	7.52	9.05	7.67
10	4	7.32	8.98	7.06
12	4	9.26	10.66	8.77
20	6	16.90	17.96	14.47
30	10	26.65	27.51	20.38

The reason for this particular finite size effect is as follows. In the charged  $P^\pm$  chains, there occurs a single carrier, a vacancy or a double occupancy within Hubbard and extended Hubbard models. Even for large Coulomb interactions, this carrier can be delocalized over the entire chain (see Fig. 6). In contrast, in the  $1^1B_u$  or the  $n^1B_u$  (and also in the  $n^3B_u$ ) both the vacancy and the double occupancy are present, and hence the overall space left for the delocalization of any one carrier is considerably smaller. This reduced delocalization in the neutral chain increases the energies of the  $1^1B_u$  states (and also of the CT triplet state,  $n^3B_u$ ) [40]. Furthermore, the “squeezed” nature of the wavefunctions of the excited states of neutral chains implies that the matrix elements of the type  $\langle P^+P^- | H_{\text{inter}} | 1^1A_g 1^1B_u \rangle$  (and the corresponding matrix elements in the triplet channels) are also modified strongly in short chains. These finite size effects are larger in the higher energy states than in the lowest excitons (since only higher energy CT states have delocalized character in the long chain limit), and hence it is to be expected that the calculated yields of the higher energy singlet and triplet excitations for *realistic* Coulomb parameters in short chains may not be representative of the results expected for long chains. In order to understand long chain behavior, we will have to minimize the relative difference in the characters of the neutral excited states and the charged polaron states. Since it is not possible to enhance the delocalizations of the double occupancy and the vacancy of the  $1^1B_u$  and the  $n^3B_u$ , we will go to the opposite limit of very strong Coulomb correlations, where the  $1^1B_u$ , the  $n^3B_u$  and the  $P^\pm$  are all nearly *equally localized*. As shown previously in the context of optical nonlinearity, the strong Coulomb interaction limit for short chains can mimic the behavior of long chains with

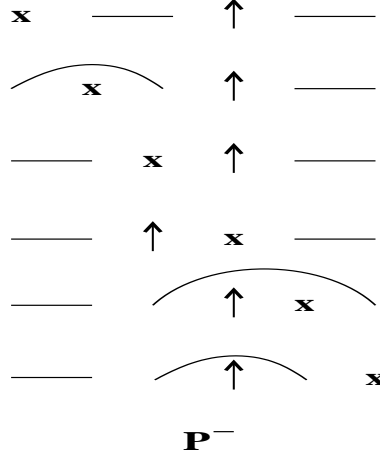


FIG. 6.: A series of valence bond diagrams in which there occurs delocalization of the doubly occupied site (denoted by  $x$ ) in polaron  $P^-$  from left to right. The up arrow corresponds to an unpaired electron and a line between two sites denotes singlet spin-pairing of the singly occupied orbitals at the sites. In case of polaron  $P^+$ , the site with double occupancy ( $x$ ) is replaced by an empty orbital. In excited states containing both the double occupancy and the vacancy in short chains, delocalization of each is considerably reduced, as they cannot pass one another without first going through a virtual state with mutual annihilation.

intermediate Coulomb interactions [24].

## 6.4 Hubbard model simulations

We consider  $H_{\text{intra}}$  as the simple Hubbard model ( $V_{ij} = \epsilon_i = 0$  in Eq. 5) with  $t_{ij} = t(1 \pm \delta)$ ,  $t = 1$  and  $\delta = 0.2$ . For  $H_{\text{inter}}$  we choose the  $V_{ij} = X_{\perp} = 0$  limit of Eq. 7, and  $t_{\perp} = 0.1$ . In what follows, we will no longer discuss the oscillatory behavior of  $I_{mn}(t)$ , but will instead present the total yields  $Y_{mn}$ , obtained by integrating  $I_{mn}(t)$  over the total duration of time evolution. As discussed in the previous subsection, within the simple Hubbard model  $E(1^1B_u) > E(P^+) + E(P^-)$  and we do not expect any significant yield of  $1^1B_u$  states higher than the  $1^1B_u$ . On the other hand, with increasing  $U$  the triplet energy difference  $\Delta E(1^3B_u) = E(P^+) + E(P^-) - E(1^3B_u)$  increases rapidly, while based on the discussions in section 4 we expect  $\Delta E(n^3B_u) = E(P^+) + E(P^-) - E(n^3B_u)$  to decrease. Simultaneously, there occur many different triplet states below  $E(P^+) + E(P^-)$ . It is of interest then to evaluate the yields of all these triplet states and to determine whether or not the results based on the PPP Hamiltonian survive for very strong Coulomb interactions. As indicated below, by simultaneously monitoring the  $Y_{mn}$ , the energy difference between the final and initial states, and the corresponding matrix elements, we are able to obtain a useful mechanistic viewpoint of the e-h recombination.

In Figs. 7(a) and (b) we have summarized our results for the singlet channel. In spite of a thorough search, we did not find significant yield for any  $1^1B_u$  state other than

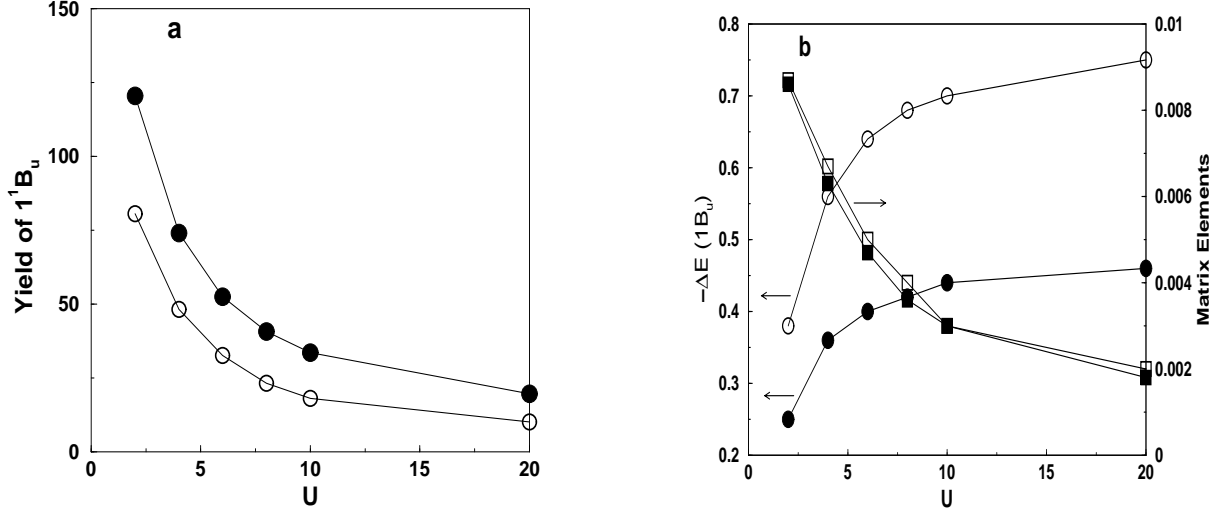


FIG. 7. (a) Yield of  $1^1B_u$  as a function of  $U$  for a pair of butadienes (open circles) and for a pair of hexatrienes (filled circles). (b) Energy difference  $\Delta E(1^1B_u)$  (see text) and  $\langle P^+P^- | H_{\text{inter}} | 1^1A_g 1^1B_u \rangle$  as functions of  $U$  for a pair of butadienes (open circles and open squares respectively) and for a pair of hexatrienes (filled circles and filled squares respectively).

the  $1^1B_u$ . The yield for the  $1^1B_u$  decreases with  $U$  for both  $N = 4$  and  $6$ , as shown in Fig. 7(a). We have also evaluated the energy difference  $\Delta E(1^1B_u) = E(P^+) + E(P^-) - E(1^1B_u)$  as a function of  $U$ . As shown in Fig. 7(b),  $|\Delta E(1^1B_u)|$  which are in units of  $t$  increases and the matrix element  $\langle P^+P^- | H_{\text{inter}} | 1^1A_g 1^1B_u \rangle$  decreases with increasing  $U$ , suggesting that the yield scales as  $\langle P^+P^- | H_{\text{inter}} | 1^1A_g 1^1B_u \rangle / |\Delta E(1^1B_u)|$ , as would be true in a tunneling process. We have confirmed this scaling behavior based on our data. Interestingly, the matrix elements for  $N = 4$  and  $6$  are nearly the same, and the higher yield in the longer chain is a simple consequence of the smaller  $|\Delta E(1^1B_u)|$ .

As expected, the behavior in the triplet channel is more complex. First of all, no  $3^3B_u$  state other than the  $1^3B_u$  and the  $n^3B_u$  are generated in significant amounts, although several triplet states are found below the  $1^1B_u$  state for large  $U$ . This may be an artifact of the symmetry imposed by us on the two-chain model system (see section 7). More importantly, with increasing  $U$ , dominant triplet yield switches from the  $1^3B_u$  state to the  $n^3B_u$  state, as seen in Fig. 8 (a) ( $n = 5$  and  $7$  in butadiene and hexatriene, respectively). In Fig. 8(b) we have shown the behavior of  $|\Delta E(1^3B_u)|$  and  $|\Delta E(n^3B_u)|$  (where the energy differences in units of  $t$  are again with respect to  $E(P^+) + E(P^-)$ ), as well as the matrix elements  $\langle P^+P^- | H_{\text{inter}} | 1^1A_g 1^3B_u \rangle$  and  $\langle P^+P^- | H_{\text{inter}} | 1^1A_g n^3B_u \rangle$  for the case of  $N = 4$  (the behavior of these quantities for  $N = 6$  are identical). The rapid increase of  $\Delta E(1^3B_u)$  and the decrease of  $\langle P^+P^- | H_{\text{inter}} | 1^1A_g 1^3B_u \rangle$ , shown in Fig. 8(b), explain the rapid decrease in the  $1^3B_u$  yield seen in Fig. 8(a).  $E(n^3B_u)$  is higher than  $E(P^+) + E(P^-)$  for all values of  $U$  (which as pointed out in the above, is a finite size

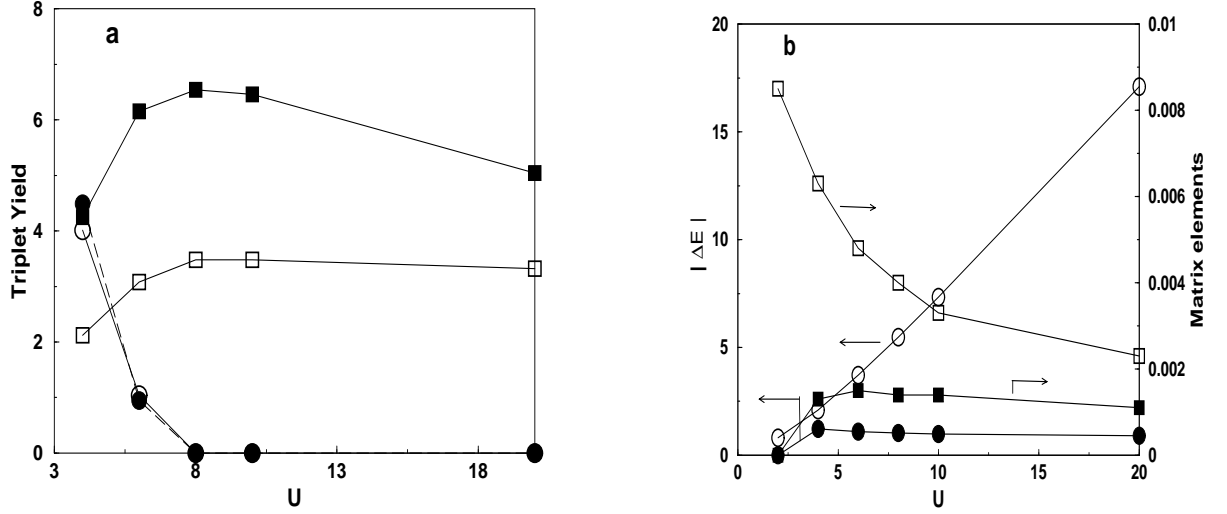


FIG. 8. (a) Yields for the  $1^3B_u$  and  $n^3B_u$  as a function of  $U$ , for a pair of butadienes (open circles and open squares respectively) and for a pair of hexatrienes (filled circles and filled squares respectively). (b)  $|\Delta E(j^3B_u)|$  and  $\langle P^+P^- | H_{\text{inter}} | 1^1A_g j^3B_u \rangle$  versus  $U$  for  $j = 1$  (open circles and open squares) and  $j = n$  (filled circles and filled squares) for a pair of butadienes. Unlike in Fig. 7, we have plotted here the absolute energy differences, as the  $n^3B_u$  can occur both above and below the  $|P^+P^- \rangle$  due to finite size effects.

effect) and the  $|\Delta E(n^3B_u)|$  decreases very slowly with increasing  $U$ . The matrix element  $\langle P^+P^- | H_{\text{inter}} | 1^1A_g n^3B_u \rangle$  remains almost a constant over the complete range of  $U$  we have studied. Thus the initial increase in the yield of the  $n^3B_u$  followed by its saturation is expected from the behavior of  $\langle P^+P^- | H_{\text{inter}} | 1^1A_g n^3B_u \rangle / |\Delta E(n^3B_u)|$ . Interestingly,  $\langle P^+P^- | H_{\text{inter}} | 1^1A_g 1^3B_u \rangle$  continues to be larger than  $\langle P^+P^- | H_{\text{inter}} | 1^1A_g n^3B_u \rangle$  even in the region where the yield of the  $n^3B_u$  is higher, indicating once again that both the matrix element and the energy difference between the initial and final states determine the yield in any given channel. Taken together, the results of Figs. 8 also suggest that in the triplet channels, matrix elements favor higher yield for the  $1^3B_u$ , but energetics favor higher yield for the  $n^3B_u$ .

The time-dependent perturbation theory [49] shows that the transition probability to a specified excited state  $|k \rangle$  from an initial state  $|i \rangle$  is given by

$$P_{i \rightarrow k} = \left| \frac{\langle k | H' | i \rangle}{E_k - E_i} \right|^2 \quad (11)$$

In this spirit, we compute the transition probability to all the dominant singlets as well as triplets. From these transition probabilities, we compute  $\eta_{TP}$  for various values of the Hubbard parameter  $U$ . We also compute  $\eta_D$  from the yields to all the singlet and triplet states obtained from our dynamical simulations. These two are shown as a function of  $U$  in Fig. 9 for a pair of hexatrienes. Similar behavior is also seen for a pair

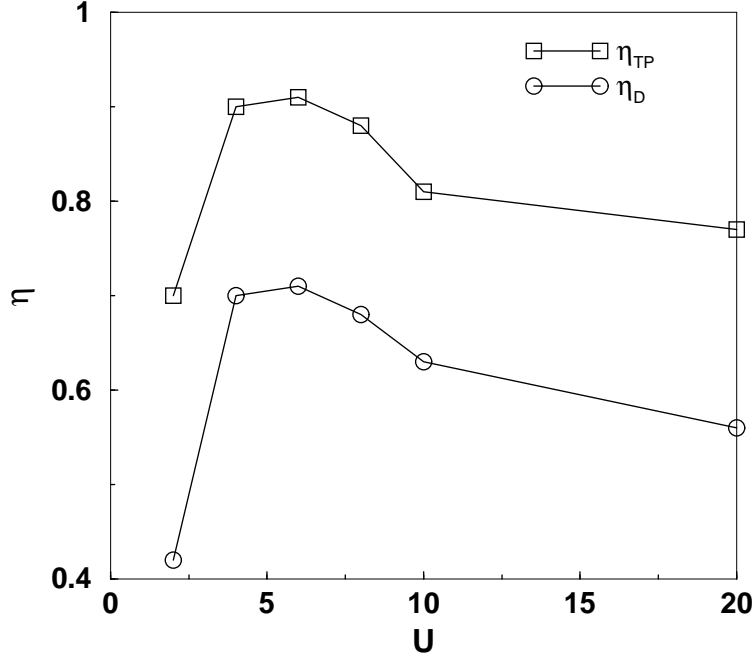


FIG. 9. Variation of  $\eta$  as a function of  $U$  for a pair of hexatrienes.

of butadienes. We note that the two different approaches give qualitatively the same behavior. This clearly vindicates our focus on the matrix elements of the interchain interactions and the energy differences between the initial and final states.

Although the above finite size calculations by themselves have limited scope, we believe that they are quite instructive. The behavior in the triplet channel clearly shows the bifurcation of the reaction paths, with the relative weights of the two paths being a strong function of the Coulomb parameter. The energy difference factor is large for the  $1^3B_u$  (which has the larger matrix element with the initial reactant state), while the matrix element is smaller for  $n^3B_u$  and the energy difference is smaller. The  $1^1B_u$  has both a large matrix element (as the  $1^3B_u$ ) as well as a small energy difference (as the  $n^3B_u$ ), and hence its yield is larger than the overall triplet yield which is the sum total of the yields of the  $1^3B_u$  and the  $n^3B_u$ . We believe that this particular result continues to be valid qualitatively for long chains with realistic Hubbard  $U$ .

## 6.5 Simulations within the extended Hubbard model

The simple Hubbard model does not lead to exciton formation and the singlet yield is limited to the  $1^1B_u$ . In order to see the bifurcation of the e-h reaction path in the singlet channel, one therefore has to work with  $H_{\text{intra}}$  corresponding to extended Hubbard models which support an excitonic electron structure. For moderate Coulomb interactions, as in the PPP model, the bifurcations are washed out due to the finite size effects discussed in section 6.3. We perform our calculations again for very strong

Coulomb interactions in  $H_{\text{intra}}$ , where finite size effects are minimized due to extreme localization, both in the charged and neutral systems. Furthermore, we restrict the intersite Coulomb interactions to nearest neighbors only, to minimize the particle-hole separation in the  $1^1B_u$  exciton state and generate very strongly bound exciton. This procedure ensures that there exist distinct delocalized CT states above the exciton even in short chains (see section 4). We have again chosen  $X_\perp = 0$  and  $t_\perp = 0.1$  in  $H_{\text{inter}}$ . In order to be consistent with nonzero intrachain intersite Coulomb interaction, we have now included interchain  $V = 10\%$  of intrachain  $V$ .

The results of our calculations are shown in Table 3, where we have listed the yields of the two dominant singlet ( $1^1B_u$  and  $n^1B_u$ ) and dominant triplet ( $1^3B_u$  and  $n^3B_u$ ) states, the energy differences  $\Delta E(j^1B_u)$  and  $\Delta E(j^3B_u)$  ( $j = 1$  and  $n$ ), defined as before with respect to  $E(P^+) + E(P^-)$ , and the relevant matrix elements of  $H_{\text{inter}}$  between the initial and various final states. Several conclusions emerge from these data.

(1) For such large Coulomb interactions the  $n^3B_u$  is (for moderate  $U = 10$ ,  $V = 3$  and 4) energetically close to the initial state even as the  $n^1B_u$  is considerably higher in energy (we have already argued that the latter is a finite size effect [26]). As in the previous subsection, the bifurcation in the triplet channel leads to a very high yield of the  $n^3B_u$ . Differently from the previous case though, the exciton character of the  $1^1B_u$  ensures a large  $\Delta E(1^1B_u)$  in the present case, and hence a small yield of the  $1^1B_u$ . Thus in this narrow regime of Coulomb interactions, the triplet yield dominates over the singlet yield. This is an artifact of our restriction to short chains, as explained below.

(2) As the Coulomb interactions are increased further, the bifurcation in the singlet channel reaction path sets in and in this case the  $n^1B_u$  yield dominates over that of the  $1^1B_u$ . Indeed in this region the  $\Delta E(n^3B_u)$  is moderately large once again even as  $\Delta E(n^1B_u)$  is small (though still negative). Thus in the limit of very large Coulomb interactions the overall singlet yield again dominates over the triplet yield, as within the PPP model, with the difference that here in both the spin channels the higher energy state dominates over the corresponding lower energy state.

(3) Matrix elements of  $H_{\text{inter}}$  between initial and final states are not independent of the energy difference between them, – smaller the energy difference larger is the matrix element. This makes understanding the finite size effects extremely important, since in short chains where the higher energy singlet and triplet states are much too high in energy, matrix elements leading to these states are *simultaneously* small, thereby reducing the overall yields to these states. In both singlet and triplet channels, we expect the bifurcations of the reaction paths to play important roles in the long chain limit.

(4) Finally, we note that even as the energy differences between the initial polaron-pair state and higher (lower) energy final states become small (large), the relevant matrix elements continue to be large for the lower states  $1^1B_u$  and  $1^3B_u$ . We believe that this will continue to be true in the long chain limit, the implication of which is that the matrix elements favor the lower excitons, while the smaller energy difference favors the higher energy CT states. This result is the same as that observed in the

triplet channel for the simple Hubbard model. The true sum total yields in either spin channel is therefore very difficult to calculate directly, and proper implications of the above data should be sought.

Table 3: *The energy differences, matrix elements and yields of singlet and triplet  $B_u$  states for various values of  $U$  and  $V$  parameters of  $N=6$  with  $H_{\text{intra}}$  as the extended Hubbard model. For each set of  $U$  and  $V$ , the first row corresponds to  $S = 0$  and the second row corresponds to  $S = 1$ . The total singlet to triplet yield ratio is small at the top but high at the bottom of the table. All energies are in units of  $t$ .*

$U$	$V$	$\Delta E(1B_u)$	$\Delta E(nB_u)$	$H'_{P^+ \otimes P^- ; G \otimes 1B}$ ( $10^{-3}$ )	$H'_{P^+ \otimes P^- ; G \otimes nB}$ ( $10^{-3}$ )	$Y(1B)$	$Y(nB)$
10	3	0.84	-1.53	4.12	0.35	16.84	
		6.93	-0.14	3.21	1.64	0.18	77.36
10	4	1.83	-1.65	3.49	0.53	3.00	
		6.64	0.27	3.39	1.45	0.21	66.67
12	4	1.60	-1.40	3.33	0.54	4.27	
		8.74	0.50	2.88	1.41	0.11	17.88
20	6	3.13	-1.06	2.10	0.64	0.65	0.87
		16.58	2.43	2.03	0.92		0.43
30	10	6.86	-0.86	1.53	0.59	0.11	0.76
		26.42	6.26	1.70	0.68		

## 7 Discussion and conclusions

Although our calculations are for finite systems, they have the advantage of being exact. Based on our experience [24], we believe that true long chain behavior for realistic Coulomb interactions can be obtained by “grafting together” the different pieces of information discussed in sections 6. The interpretation of the PPP model calculations is obvious: although  $|\langle 1^1A_g \cdot 1^1B_u | H_{\text{inter}} | P^+P^- \rangle_S| \sim |\langle 1^1A_g \cdot 1^3B_u | H_{\text{inter}} | P^+P^- \rangle_T|$  with these parameters, the proximity of the  $S = 0$  final state to the initial polaron-pair state relative to the  $S = 1$  final state favors the singlet, thereby leading to  $\eta$  considerably larger than 0.25 [13, 14]. No significant yield to higher energy states are obtained within the PPP model at our chain lengths, but as we have shown, this is because the magnitudes of the matrix elements between initial and final states depend on the energy differences between them, and at these short chain lengths, the relevant energy differences are too large. Thus the PPP model results cannot be thought of as complete. The results in section 6.4 are very instructive. The relatively large (small) energy difference between the  $1^3B_u$  ( $n^3B_u$ ) and the initial state composed of the polaron pairs that occurs here for large Hubbard  $U$  is exactly what is expected at long chain lengths for intermediate  $U$ . We expect then that in long chains dominant singlet yield to the  $1^1B_u$  and dominant triplet yield to the  $n^3B_u$ . The continuing higher yield of the singlet, even when compared to the total triplet yield, is then significant. The reason for the relatively lower triplet yield can be understood from Fig. 8(b), – even as  $|\langle 1^1A_g \cdot 1^3B_u | H_{\text{inter}} | P^+P^- \rangle_T|$  decreases with  $U$ , it remains larger than  $|\langle 1^1A_g \cdot n^3B_u | H_{\text{inter}} | P^+P^- \rangle_T|$ . In contrast, the  $1^1B_u$  remains energetically proximate to  $|P^+P^- \rangle_S$ , and hence the matrix element in the singlet channel also continues to be larger. The resultant large  $\eta$  within simple Hubbard models is therefore expected even in the long chain limit.

The behavior within the extended Hubbard model is only slightly more complex. Once again, we believe that increasing Coulomb correlations at fixed  $N$  is qualitatively equivalent to increasing  $N$  at fixed Coulomb correlations, since both have the same effect on the order and proximities of the most relevant energy states. We have not included the results for smaller  $U$ ,  $V$  in Table 2, because at these parameters the behavior continues to be similar to that within the PPP model, i.e., the yields are dominated by the lowest  $S = 0$  and 1 excitons, with  $\eta > 0.25$ . With stronger Coulomb interactions, in both the singlet and triplet channels the yield shifts from the lowest excitons to the higher  $nB_u$  states. Nevertheless,  $\eta$  is predicted to be greater than 0.25 for most of the parameter space. Unfortunately, we are unable to demonstrate the gradual shift from lower energy to higher energy products as would occur upon increasing  $N$  at fixed Coulomb correlations: our reaction products are either the lower energy states or the higher energy ones. We believe that the true long chain behavior is very likely a “superposition” of the calculated results for moderate and strong Coulomb interactions, viz., larger matrix elements with the lower states as final states favoring these, while proximities in energy favoring the higher CT states. For systems with relatively small singlet exciton binding energies, in the long chain limit we expect the yield in the singlet channel to be dominated by the  $1^1B_u$ , as in the simple Hubbard model. For



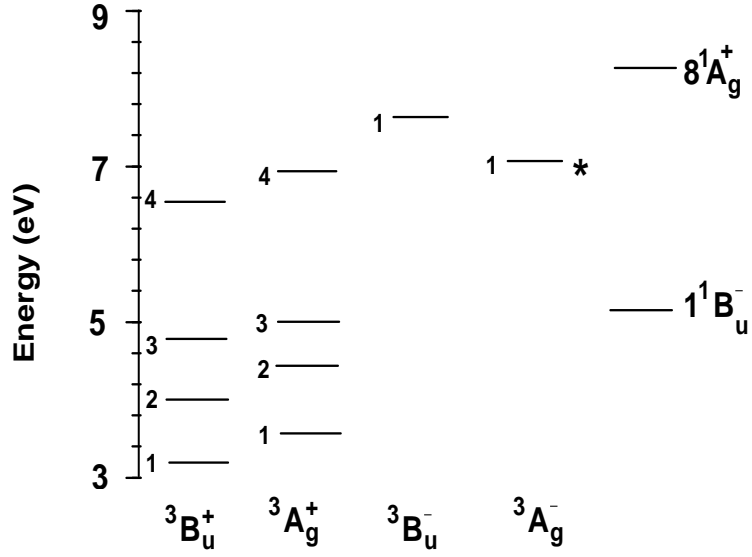


FIG. 10. The triplet energy spectrum between the  $1^3B_u^+$  and  $1^3A_g^-$  in a  $N = 12$  chain relative to the singlet ground state, within the PPP-Ohno Hamiltonian. Different symmetry subspaces are shown separately. State marked by asterisk is dipole-coupled to the  $1^3B_u^+$ . The  $1^1B_u^-$  and the  $m^1A_g^+$  ( $m = 8$  in  $N = 12$ ) are also included.

systems with large singlet exciton binding energy, it is conceivable that the  $n^1B_u$  and the  $n^3B_u$  both make significant contributions. The relative yield of the  $1^3B_u$  in these systems should be very small, and as a consequence we expect again the overall  $\eta$  to be large. To summarize then, what varying chain lengths, Coulomb parameters and exciton binding energies do is redistribute the overall yields within each spin channel between the lowest exciton and the higher energy CT state. However, even after this redistribution  $\eta$  remains greater than 0.25. Clearly, completely convincing proof of the above conjecture would require long chain calculations that can treat low and high energy states as well as the polaron-pair states of long chains with high precision. We are pursuing density matrix renormalization group calculations currently to test the ideas posed in the above.

One apparent surprise in our results is the overall limitation to the  $1^3B_u$  and the  $n^3B_u$  as products in the triplet channel e-h recombination. This is surprising, given that there exist so many covalent triplet states between the  $1^3B_u$  and the  $n^3B_u$  even in short chains (Fig. 10).

Indeed, if these triplets were generated, in principle  $\eta$  could have reached values smaller than 0.25. One reason these triplets are not generated within our calculations is because of the artificial mirror plane symmetry that we have imposed between the two polyene chains, as a consequence of which even the charge-separated polaron-pair states have  $B_u^-$  and  $B_u^+$  symmetries in singlet and triplet spin spaces, respectively, and the interchain hop maintains these symmetries. All low to intermediate energy triplets

that belong to symmetry subspaces different from the  ${}^3B_u^+$  are thereby excluded. There do exist, however,  ${}^3B_u^+$  states above the  $1^3B_u$  but below the  $n^3B_u$ , and even these are not generated in significant amounts over a broad region of the parameter space. We are currently pursuing exact calculations with all possible relative orientations between the two molecular components. While these calculations will obviously generate singlets and triplets belonging to all possible symmetry subspaces, we believe that they will demonstrate the existence of approximate “sum rules”, i.e., the total yield in each spin channel remains nearly conserved, and that the total yields are close to what we have already found in our current calculations.

Finally, we address the issue of electron-phonon interactions, ignored in our calculations. Electron-phonon interactions play a dominant role in theories of e-h recombination in which intermolecular charge-transfer leads to higher energy singlet and triplets only, and differences in cross-sections arises from differences in structural relaxations to the lowest excitons [15, 16]. As we have pointed out elsewhere, these theories ignore triplet states in between the high energy charge-transfer state and the lowest triplet, and such triplets should definitely be involved in nonradiative relaxation [21]. Inclusion of these intermediate triplets will enhance the triplet relaxation and wipe out all differences between singlet and triplet relaxations that give the difference between singlet and triplet yields within the above theories. The only way electron-phonon interactions can influence the singlet:triplet yield within our picture is if these interactions change substantively the relative energies of the most relevant states. It has been claimed by Conwell, for example, that the relaxed polaron energies  $E(P^+) + E(P^-)$  can be considerably below the  $E(n^1B_u)$  that is observed in nonlinear optical experiments [50]. This has, however, not been substantiated by any calculations, and we are currently investigating this possibility.

## 8 Acknowledgments

Work in Bangalore was supported by the CSIR, India and DST, India, through /INT/US (NSF-RP078)/2001. Work in Arizona was supported by NSF-DMR-0101659, NSF-DMR-0406604 and NSF-INT-0138051. We are grateful to our experimental colleagues Z.V. Vardeny and M. Wohlgenannt for numerous stimulating discussions. S.M. acknowledges the hospitality of the Indian Institute of Science, Bangalore, where this work was completed.

## References

- [1] Y. Cao, I. D. Parker, G. Yu, C. Zhang, and A. J. Heeger, *Nature (London)* **397**, 414 (1999).
- [2] P. K. H. Ho, J. S. Kim, J. H. Burroughes, H. Becker, S. F. Y. Li, T. M. Brown, F. Cacialli, and R. H. Friend, *Nature (London)* **404**, 481 (2000).

- [3] J. S. Wilson, A. S. Dhoot, A. J. A. B. Seeley, M. S. Khan, A. Köhler, and R. H. Friend, *Nature (London)* **413**, 828 (2001).
- [4] M. Wohlgenannt, K. Tandon, S. Mazumdar, S. Ramasesha, and Z. V. Vardeny, *Nature (London)* **409**, 494 (2001).
- [5] A.S. Dhoot , and N.C. Greenham, *Adv. Mater.* **14**, 1834 (2002).
- [6] M. Wohlgenannt, X. M. Jiang, Z. V. Vardeny, and R. A. J. Janssen, *Phys. Rev. Lett.* **88**, 197401 (2002).
- [7] T. Virgili, G. Cerullo, L. Luer, G. Lanzani, C. Gadermaier , and D.D.C. Bradley, *Phys. Rev. Lett.* **90**, 247402 (2003).
- [8] M. A. Baldo, D. F. O'Brien, M. E. Thompson, and S. R. Forrest, *Phys. Rev. B* **60**, 14422 (1999).
- [9] M. Segal, M . A. Baldo, R. J. Holmes, S. R. Forrest, Z. G. Soos, *Phys. Rev. B* **68**, 075211 (2003).
- [10] G. Li, C.H. Kim, P.A. Lane , and J. Shinar *Phys. Rev. B* **69** 165311 (2004).
- [11] Z. Shuai, D. Beljonne, R. J. Silbey, and J. L. Bredas, *Phys. Rev. Lett.* **84**, 131 (2000).
- [12] A. Ye, Z. Shuai, and J. L. Bredas, *Phys. Rev. B* **65**, 045208 (2002).
- [13] Kunj Tandon, S. Ramasesha, S. Mazumdar, *Phys. Rev. B* **67**, 045109 (2003).
- [14] S. Ramasesha, S. Mazumdar, Kunj Tandon , and Mousumi Das , *Synthetic Metals*, **139**, 917 (2003).
- [15] T.-M. Hong , and H.-F. Meng, *Phys. Rev. B* **63**, 075206 (2001).
- [16] M. N. Kobrak , and E. R. Bittner, *Phys. Rev. B.* **62** 11473 (2000). S. Karabunarliev and E.R. Bittner, *J. Chem. Phys.* **119**, 3988 (2003).
- [17] M. Kasha, *Discuss. Faraday Soc.* **9**, 14, (1950).
- [18] L.C. Lin *et al.*, *Phys. Rev. Lett.* **90**, 036601 (2003).
- [19] R. Österbacka, *Phys. Rev. Lett.* **91**, 219701 (2003).
- [20] A.S. Dhoot , and N.C. Greenham, *Phys. Rev. Lett.* **91**, 219702 (2003).
- [21] S. Mazumdar, Mousumi Das, S. Ramasesha, cond-mat/0310456.
- [22] R. Pariser and R. G. Parr, *J. Chem. Phys.* **21**, 466 (1953). J. A. Pople, *Trans. Faraday Soc.* **49**, 1375 (1953).
- [23] Z. G. Soos and S. Ramasesha, *Phys. Rev. B* **29**, 5410 (1984).

- [24] D. Guo, S. Mazumdar, S. N. Dixit, F. Kajzar, F. Jarka, Y. Kawabe and N. Peyghambarian, *Phy. Rev. B* **48**, 1433 (1993).
- [25] S. Abe, J. Yu , and W. P. Su, *Phys. Rev. B* **45**, 8264 (1992).
- [26] A. Race, W. Barford and R. J. Bursill, *Phy. Rev. B* **64**, 35208 (2001).
- [27] S. Ramasesha, Swapan K. Pati, Z. Shuai, and J. L. Bredas, *Adv. Quantum Chem.*, Academic Press, London, **38** 121, (2000).
- [28] G. Weiser, *Phy. Rev. B* **45**, 14076 (1992).
- [29] J.M. Leng, S. Jeglinski, X. Wei, Z.V. Vardeny, R.E. Benner, F.Y. Guo and S. Mazumdar, *Phys. Rev. Lett.* **72**, 156 (1994).
- [30] M. Liess, S. Jeglinski, Z. V. Vardeny, M. Ozaki, K. Yoshino, Y. Ding and T. Barton, *Phys. Rev. B* **56**, 15712 (1997).
- [31] J. W. Blatchford, S. W. Jessen, L. B. Lin, J. J. Lih *et al.* *Phys. Rev. Lett.* **76**, 1513 (1996).
- [32] M. B. Sinclair, D. McBranch, T. W. Hagler, A. J. Heeger , *Synth. Metals*, **50**, 593 (1992).
- [33] I. D. W. Samuel, F. Raksi, D. D. C. Bradley, R. H. Friend *et al.* , *Synth. Metals*, **55**, 15 (1993).
- [34] J. M. Leng, S. Jeglinski, X. Wei, R.E. Benner, Z.V. Vardeny, F.Y. Guo and S. Mazumdar, *Phys. Rev. Lett.* **73**, 3180 (1994).
- [35] J. W. P. Hsu, M. Yan, T. M. Jedju, L. J. Rothberg, B. R. Hsieh, *Phys. Rev. B*, **49**, 712 (1994).
- [36] M. Yan, L. J. Rothberg, F. Papadimitrakopoulos, M. E. Galvin, T. M. Miller, *Phys. Rev. Lett.* **72**, 1104 (1994).
- [37] Y. Shimoï and S. Mazumdar, *Synth. Metals*, **85**, 1027 (1997).
- [38] Z. G. Soos, S. Ramasesha, D. S. Galvao, *Phys. Rev. Lett.* **71**, 1609 (1993).
- [39] M. Chandross and S. Mazumdar, *Phys. Rev. B* **56**, 15712 (1997).
- [40] Z. Shuai, J. L. Bredas, Swapan K. Pati and S. Ramasesha, *Phys. Rev. B* **56**, 9298 (1997).
- [41] A. Kadashchuk, A. Vakhnin, I. Blonski, D. Beljonne, Z. Shuai, J. L. Bredas, V. I. Arkhipov, P. Heremans, E. V. Emelianova, and H. Bäessler, *Phys. Rev. Lett.* **93**, 66803 (2004).
- [42] K. Ohno, *Theor. Chim. Acta.*, **2**, 219 (1964).

- [43] J. T. Gammel and D. K. Campbell, Phys. Rev. Lett. **60**, 71 (1988), D. K. Campbell, J. T. Gammel and E. Y. Loh, Phys. Rev. B **42**, 475 (1990).
- [44] M. J. Rice, Yu. N. Gartstein, Phys. Rev. B **53**, 10764 (1996).
- [45] J. Crank and P. Nicholson, Proc. Cambridge Philos. Soc., **43**, 50 (1947).
- [46] R. Varga, Matrix Iterative Analysis, Prentice-Hall Inc., New Jersey (1962).
- [47] I. I. Rabi, Phys. Rev. B **51**, 652, (1937).
- [48] L. Allen and J. H. Eberly, Optical Resonance and Two Level Atoms, Dover (1987).
- [49] Eugen Merzbacher, *Quantum Mechanics*, Wiley, New York, 503 (1999).
- [50] E.M. Conwell in *Organic Electronic Materials*, edited by R. Farchioni and G. Grosso (Springer-Verlag, Berlin, 2001), pp. 127-180.

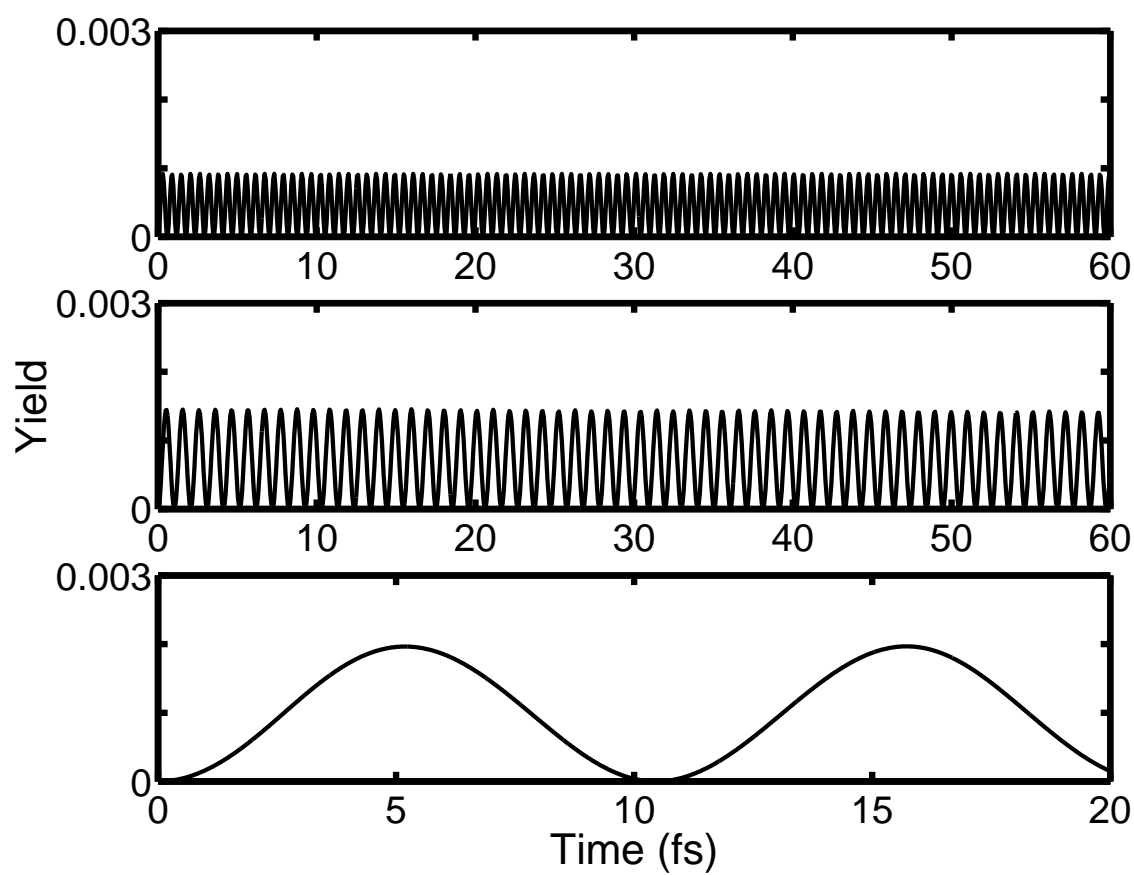


Figure 3 (c)

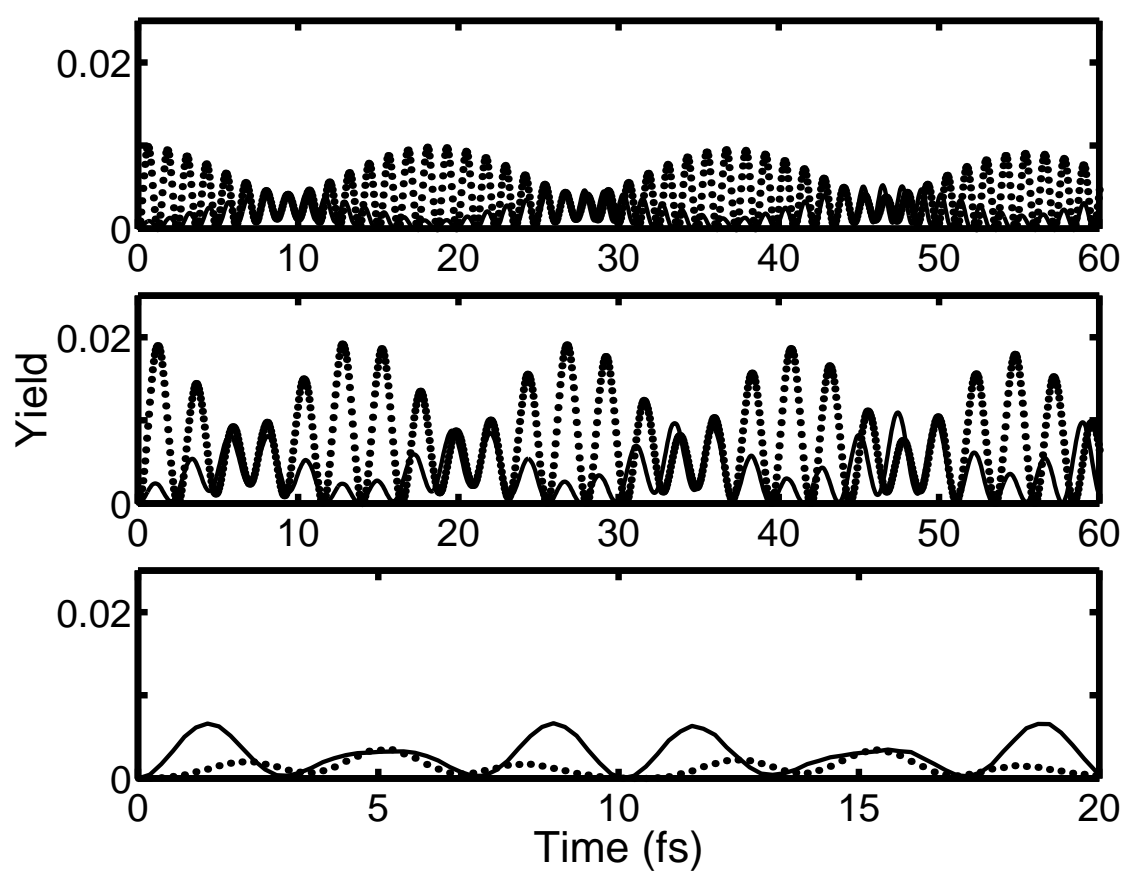


Figure 3 (d)

